




# Burning Behavior Analysis in Meso and Large-Scale Oil Slick Fires With and Without Waves Using Outdoor Gas Emission Sampling (OGES) System

Hsin-Hsiu Ho <sup>\*</sup>, Fire Protection Engineering, Worcester Polytechnic Institute, 100 Institute Road, Worcester, MA 01609, USA

Kemal S. Arsava, Cold Regions Research and Engineering Laboratory (CRREL), US Army Corps of Engineers, 72 Lyme Rd, Hanover, NH 03755, USA

Ali S. Rangwala, Fire Protection Engineering, Worcester Polytechnic Institute, 100 Institute Road, Worcester, MA 01609, USA

**Received:** 28 September 2021/**Accepted:** 9 March 2022/**Published online:** 26 March 2022

**Abstract.** A new Outdoor Gas Emission Sampling (OGES) system was developed to serve as a low-cost alternative to expensive industrial gas sampling equipment. This research showed its effectiveness in sampling a smoke plume from multiple points simultaneously, obtaining gas concentration curves for common products of combustion such as CO<sub>2</sub> and CO in meso-scale experiments. The optimal height for combustion product sampling was determined based on a variety of factors, most notably CO/CO<sub>2</sub> ratio, which showed to be most consistent when located in the intermittent and plume regime of the McCaffrey plume. Large-scale field tests at U.S. Army Cold Regions Research and Engineering Laboratory (CRREL) in collaboration with the Environmental Protection Agency (EPA) demonstrated the potential of using OGES to evaluate the completeness of combustion for various fuels in a variety of settings. Oxygen Consumption (OC) and Carbon Dioxide Generation (CDG) methods in combination with plume theory results show the potential of using point sampling within a smoke plume to estimate HRR for fires that exceed the capabilities of conventional hood-based calorimeters.

**Keywords:** Heat release rate, Products of combustion, Calorimetry, Pool fire, Crude oil

## 1. Introduction

Heat release rate (HRR) is one of the most critical parameters in fire hazard evaluation [1]. Knowledge of HRR allows for further estimation of burning efficiency, convective and radiative losses, and emissions such as smoke and by-products, which may be harmful to the environment. Tsuchiya [2] summarizes multiple

---

\*Correspondence should be addressed to: Hsin-Hsiu Ho, E-mail: [hho@wpi.edu](mailto:hho@wpi.edu)



methods for determining HRR. The first is via thermal methods, which allows calculation of HRR based on specific heat ( $c_p$ ), temperature rise ( $\Delta T$ ), and mass flow rate of flue gases ( $\dot{m}$ ). The second is through gas analysis methods, which require the mass flow rate of air, fuel, and exhaust gases through a control volume. Another common method is shown in SFPE Handbook (SFPE HB) [3] using the product of mass burning rate ( $\dot{m}_{F,s}$ ) and heat of combustion ( $\Delta H_c$ ). Heat of combustion ( $\Delta H_c$ ) is defined as the enthalpy change because of reactants (fuel + oxygen) converting to products ( $\text{CO}_2 + \text{H}_2\text{O}$ ) through the process of combustion. This enthalpy change is assumed to be captured by change in  $c_p\Delta T$ . This sensible heating of air, expressed through  $c_p\Delta T$ , can be further expressed as  $\Delta H_c$ . As a result, heat of combustion is often studied and reported for different types of fuels and length scales [3].

One of the most commonly used apparatuses for quantifying HRR is through product gas calorimetry following ASTM E1354 [4]. It is used to evaluate various characteristics of materials such as HRR, effective heat of combustion, mass loss rate, and soot production. This is achieved with a gas analyzer, differential pressure probe, thermocouple, helium–neon laser, and load cell within the apparatus. The gas analyzer analyzes concentrations of combustion products within the exhaust product stream such as  $\text{CO}_2$ , CO, and  $\text{O}_2$ . The differential pressure probe calculates the flow rate of exhaust product stream within the control volume. The thermocouple measures the temperature of the exhaust product stream. The helium–neon laser is part of a smoke obscuration measuring system that analyzes soot production. The load cell monitors mass loss rate of the burning sample, obtaining mass burning rate ( $\dot{m}_{F,s}$ ).

Heat release measurements using this apparatus are based on Oxygen Consumption (OC) calorimetry [2, 5], which is an HRR quantification technique that relies on a controlled indoor laboratory environment where there is an accurate sampling of the exhaust gases. This method utilizes the assumption that a constant amount of heat is released per unit mass of oxygen consumed ( $\Delta H_{\text{O}_2}$ ), which is 13.1 kJ/g as demonstrated in a study by Huggett [6]. Based on the formulation by Tewarson, Factory Mutual (FM) Global [7] developed a similar calorimetry method in the 1970s but instead focused on the generation of  $\text{CO}_2$  and CO. In this method, HRR can be calculated from the amount of  $\text{CO}_2$  and CO produced; this is referred to as Carbon Dioxide Generation (CDG) calorimetry. For simple organic compounds, Khan et al. [8] give average energy release constants for  $\text{CO}_2$  ( $\Delta H_{\text{CO}_2}$ ) and CO ( $\Delta H_{\text{CO}}$ ) to be 13.3 kJ/g and 11.1 kJ/g respectively.

However, because of the variables required to establish HRR, this limits the size of the design fire because the entirety of the smoke plume needs to be collected to analyze the concentrations of the various exhaust gases. An amount of make-up air also needs to be provided to the burn space that is equivalent to the exhaust mass flow being extracted out the exhaust duct of the calorimeter hood. Cooper [9] states the ideal exhaust mass flow should be equal to the total mass flow of the plume for accuracy purposes.

Worcester Polytechnic Institute (WPI) possesses a large calorimeter capable of measuring a 5 MW fire at steady-state and upwards of 15 MW intermittently.

National Institute of Standards and Technology (NIST) and Factory Mutual (FM) Global currently have the largest known commercial calorimeters in the US capable of measuring a continuous 20 MW fire for up to four hours, with a hood covering dimensions of 13.8 m by 15.4 m [7]. In many cases, larger fires are required to simulate realistic fire scenarios, such as in-situ burning (ISB) of crude oil in outdoor conditions, therefore rendering a cone calorimeter setup to be impractical as the plume cross-sectional area is expected to exceed several meters [10]. Assuming an oil spill with a burn area of 100 m<sup>2</sup>, with a burning regression rate of 4 mm/min, this corresponds to a fire of around 143 MW. Cooper [9] discussed the amount of make-up air needed in an ideal calorimeter hood design based on correlations by Heskestad [11]. For a design fire of this magnitude, the estimated amount of make-up air for the burn space would be around 450 m<sup>3</sup>/s. At present, the world's largest air compressor is capable of 277 m<sup>3</sup>/s. Both diameter and HRR of this expected fire far surpass the capabilities of any known calorimeter. This current knowledge gap is where improving a method for gas emissions point sampling to estimate HRR becomes valuable.

Previous studies by Tukaew [12] and Tukaew et al. [13] at Worcester Polytechnic Institute (WPI) were performed using an early design of the Outdoor Gas Emission Sampling (OGES) system to utilize point sampling within a smoke plume from a crude oil fire. A windsock covering a large metal frame with a gas sampling ring, differential pressure probe, and type-K thermocouple was mounted on an 8 m tall tower structure to serve as the singular gas sampling point. A pulley system was incorporated to maintain the windsock within the smoke plume as much as possible. The gas sampling ring was connected to a SERVOMEX 4200 industrial gas analyzer to record the gas concentration data. Field tests performed at the United States Coast Guard (USCG) test facility at Little Sand Island in Mobile Bay, Alabama [13] showed promise of OGES but also indicated the need for improvements in the sampling system design to systematically study completeness of combustion and possibly HRR.

A proper understanding of combustion product spatial distribution within a smoke plume is required to evaluate the applicability of point sampling on estimating burning efficiency and HRR. However, prior knowledge in this aspect is somewhat lacking. Previous studies regarding combustion production spatial distribution have been centered towards indoor scenarios related to tenable conditions for occupants [14], but little research has been performed outside of this specific application. Early studies by McCaffrey [15] showed temperature and velocity distribution curves along the radial direction within a smoke plume, but no data regarding combustion product concentrations were published. Sibulkin and Malary [16] published concentration profiles of CO<sub>2</sub> and CO to study the completeness of combustion in MMA wall fires, but the focus was centered on the change in peak CO<sub>2</sub> and CO concentrations when varying the amount of oxygen on the fuel side of the flame. Tsuchiya [2] also published values for CO/CO<sub>2</sub> ratios in well-ventilated conditions, such as ASTM HRR apparatus and E-84 tunnel tests, but did not elaborate further on the practicality of such values.

The Environmental Protection Agency (EPA) has published many findings relating to gas emissions in outdoor fires [17–19]; however, the focus of such pub-

lications was related to particulates (PM) and other toxic substances released from such fires and not the completeness of combustion or HRR, which is the focus of this study. Hariharan et al. [20] observed particulate-matter emissions from liquid pool fires and fire whirls, however, similar to EPA, they emphasized cumulative release of carbon emissions (CO<sub>2</sub>, CO, and PM) rather than real-time emissions sampling.

## 2. Experimental Setup and Methods

### 2.1. Setup

*2.1.1. Sampling Apparatus Design* The original iteration of the OGES system developed by Tukaew [12] and Tukaew et al. [13] utilized a flexible windsock attached to a rigid metal frame, which would alleviate issues of combustion product accumulation within the sampling apparatus. This would allow for the differential pressure probe within the windsock to obtain a more accurate measurement of the mass flow rate through the control volume. The wind sock and frame were mounted to a pulley system which allowed for height adjustments to account for shifting winds. All gases gathered within the wind sock were transported via tubing to an industrial gas analyzer (SERVOMEX 4200 Industrial Gas Analyzer) to determine the real-time concentrations of the combustion products. It has an effective measurement range of 0–2.5% for CO<sub>2</sub>, 0–1% (0–10,000 ppm) for CO, and 0–25% for O<sub>2</sub>.

However, using the wind sock frame and gas analyzer for gas analysis and velocity measurements required long sampling tubes and wires, as well as exceeding 30 kg in weight. Furthermore, the primary assumption made for the wind sock design was that the control volume within the wind sock had the same gas concentrations as the entirety of the smoke plume. This assumption necessitates an empirical correction factor applied to mass flow rate calculations to account for the entire plume.

One method of avoiding the use of an empirical correction factor is by using multiple sampling points, the control volume and gas analysis equipment needed to be designed in a way that required lower cost than using multiple industrial gas analyzers. The elimination of long tubes and wires was also desirable; because future research with multiple simultaneous sampling points would be made more convenient with wireless monitoring that could be performed remotely. This triggered a new iteration of OGES.

A new portable design was conceived as a substitute for the industrial gas analyzer, as well as the removal of the wind sock entirely. Small, portable sensors for CO<sub>2</sub> (GasLab TX 20% CO<sub>2</sub> Sensor), CO (GasLab AlphaSense CO-AF Sensor), and O<sub>2</sub> (GasLab TX 25% Oxygen Sensor) were purchased and placed within a sealed chamber. The measurement ranges were comparable to that of the industrial gas analyzer used in the previous iteration of OGES.

To prevent soot, water vapor, and other contaminants from entering the sensor module and affecting measurements, a sampling train with the proper filters was used. The first filter, referred to as coarse particle filter, was a polyester air filter

foam often used in HVAC systems. These filters are designed to filter dust, dander, spores, and mold; and preliminary burn tests showed that they were very effective in filtering out the majority of soot particles. The foam was placed in a column to ensure that the entire system remained sealed and ambient air would not leak into the system. A 10  $\mu\text{m}$  soot filter, or fine particle filter, was connected after the foam to filter any remaining particulates. Finally, calcium sulfate desiccants (Drierite) were used to filter out water vapor before the connected air pump (4.4 lpm) transported the gases to the gas sensor module. This air pump had the same flow rate as the one used in the studies by Tukaew [12] and Tukaew et al. [13]. Figure 1a shows a flow diagram for the new OGES; Fig. 1b and c show a prototype of the gas sensor module and filter train used throughout the experiments.

Notable improvements over Tukaew [12] and Tukaew et al. [13] include size and weight, overall portability, and cost. The newfound portability of the new OGES allowed for the gas sampling ports to be fixated on any structure without the worry of compromising its integrity, as there is a 50-fold decrease in overall system weight. Another scenario was to place sampling ports within a crane (or zip line when the crane was unavailable) as shown in Fig. 5. The crane would maneuver to sample the smoke plume continuously even during wind shifts in outdoor fires. This advantage was only made possible by the size and weight reduction of the new OGES. Another limitation to the original OGES was the singular sampling point. To achieve improved results for the development of a combustion product spatial distribution model, more simultaneous sampling points are required. However, industrial gas analyzers are expensive and therefore make it impractical to purchase multiple systems while also being hindered by their lack of mobility. The use of low-cost, portable gas sensors decreases the cost

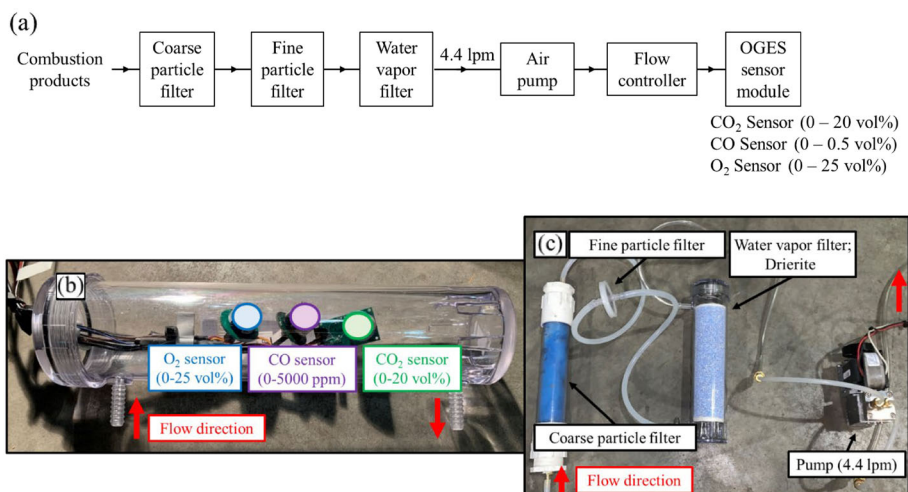


**Figure 1. New OGES, a flow diagram; b gas sensor module with CO<sub>2</sub>, CO, and O<sub>2</sub> sensors; c filter train.**

of equipment by 20-fold compared to an industrial gas analyzer, which allows for simultaneous deployment of multiple systems.

One of the most important factors to validate beforehand was the accuracy of the portable sensors compared to industrial equipment. Four-point calibration using carrier gases was performed for both the SERVOMEX and portable sensor. Results showed the signal output to be linear. Figure 2 demonstrates this linearity for the CO<sub>2</sub>, CO, and O<sub>2</sub> sensors used. Similar to ASTM E1354 [4], the SERVOMEX and OGES were zeroed and calibrated at the start of each testing day. For zeroing, 99.999% nitrogen gas was used. For calibrating, 2.50% CO<sub>2</sub>, 0.50% CO, and 20.90% O<sub>2</sub> calibration gases were used.

Validation burn experiments (75 cm pool fire) using the new OGES with the existing SERVOMEX industrial gas analyzer were performed. Figure 3 shows a flow diagram of the sampling train used during the experiments. To ensure both sampling systems obtained readings from the same sampling point, a tee was added before the flow controllers. The flow controllers going to the equipment ensured that the equipment was still receiving the correct flow rate, which was equal to the same flow rate used during calibration. Plots in Fig. 4 show that these portable gas sensors provide readings that are in good agreement with industrial equipment at gas concentrations around this range. Therefore, results reported in the latter portion of this study will be concentrations obtained from the portable sensor readings.

## 2.2. Experimental Methods

**2.2.1. Combustion Product Spatial Distribution Study** Meso-scale burn experiments were designed to investigate the spatial distribution of certain combustion products such as CO<sub>2</sub> and CO within a smoke plume. A burn pan of 75 cm in diameter was placed on a load cell to obtain mass loss rate. Two types of fuel were used for these experiments: ANS crude oil and 87-octane regular gasoline. ANS is Alaskan North Slope crude oil that is a pipeline blend from reservoirs offshore in the North Slope region of Alaska. Both fuels reached steady-state approximately 1 min after ignition. The fuel volume was 22 L, which equaled an initial fuel thickness of 5 cm. The burn pan had a depth of 6 cm. The initial

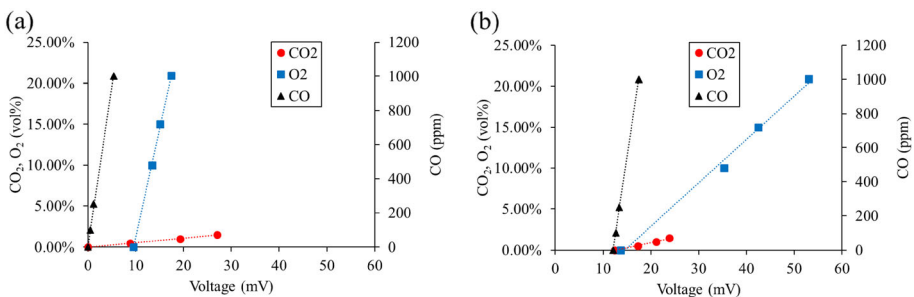


**Figure 2. Four-point calibration demonstrating linear signal output for a SERVOMEX, b portable sensors.**

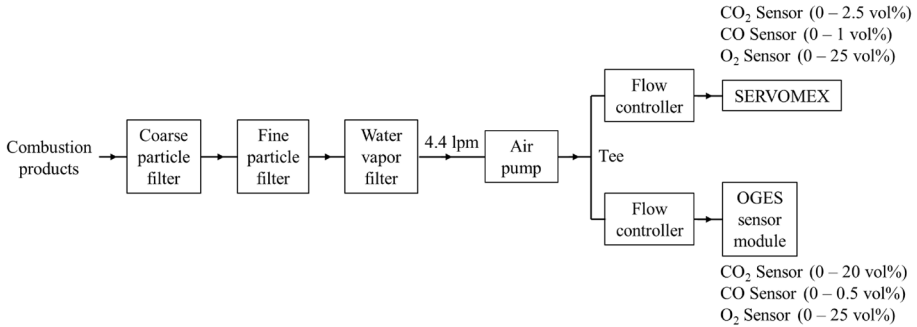


**Figure 3. Flow diagram for the SERVOMEX and the new OGES during 75 cm validation burn experiments.**

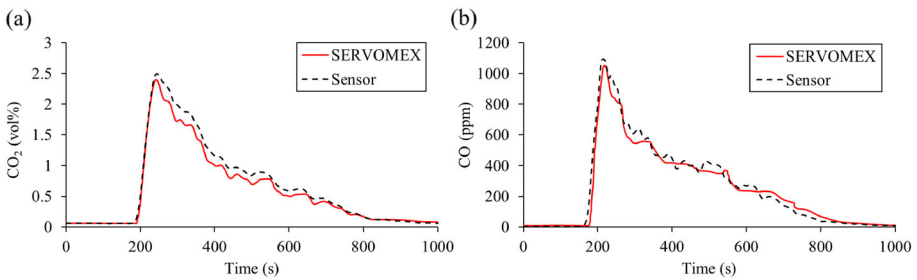


**Figure 4. Validation burn experiment plots for a CO<sub>2</sub>, b CO. Pool diameter = 75 cm; fuel = ANS crude oil; initial fuel thickness = 5 cm; fuel volume = 22 L; sampling height = 1.5 m above pool surface.**

ullage of the experiments was 1 cm and reached 6 cm towards the end of the burns. Considering the burn pan was 75 cm in diameter, lip effects were insignificant and assumed negligible.

The indoor laboratory environment at WPI provided a vertical plume that was undisturbed by wind, therefore six to nine sampling locations along the centerline of the plume could be studied simultaneously. This aspect of a vertical plume in tandem with centerline sampling points allowed for additional validation of sensor readings with plume theory correlations [11, 21] to obtain HRR.

Figure 5 illustrates the sampling locations throughout this series of experiments. Nine sampling locations were selected for the ANS crude oil experiments. Three repeat experiments were performed for all locations to ensure repeatability of gas concentrations at specific heights above the pool surface.

### 2.3. Large-Scale Field Study

A large-scale field study was performed at U.S. Army Cold Regions Research and Engineering Laboratory (CRREL) in a large wave tank with a burn area of 1.9 m by 1.7 m. 2,000 kg of salt was added to the 68,000 L of water situated within this

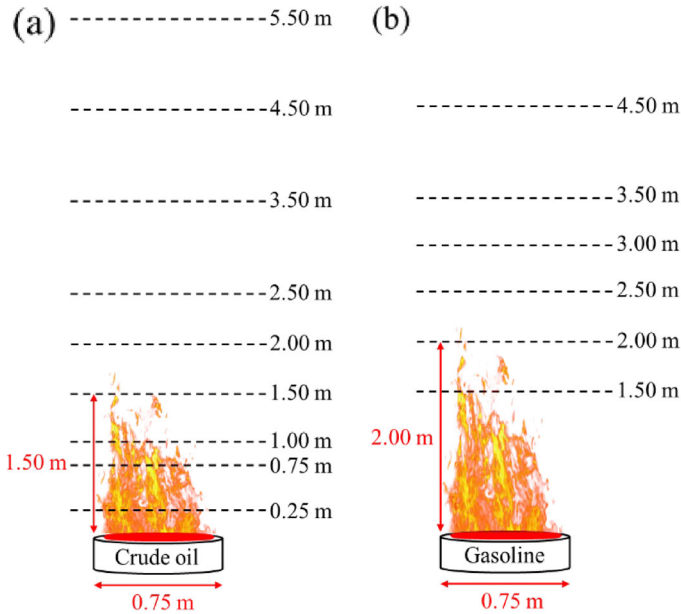


**Figure 5. Sampling locations for meso-scale 75 cm burn experiments, a ANS crude oil; b 87-octane regular gasoline.**

large wave tank to achieve a salinity of 30 parts per thousand, mimicking the salinity of the ocean. Two types of fuel were burned in the field trials: HOOPS crude oil and bunker fuel. HOOPS stands for Hoover Offshore Oil Pipeline System consisting of oils from the Diana, South Diana, Hoover, Marshall, and Madison fields in the Gulf of Mexico. The fuel was burned floating on top of water bound by a boom. Fuel volumes for HOOPS crude oil and bunker fuel were 260 L and 32 L respectively, equating to respective initial fuel thicknesses of 8 cm and 1 cm. Three wave profiles were used in the experiments (wave period; wave height): Wave 1–2.5 s, 7 cm; Wave 2–4 s, 14 cm; Wave 3–1 s, 4 cm. Wave 1 and 3 were faster but shorter waves; Wave 2 was slower but taller. OGES was set up in an attempt to continue research of completeness of combustion for various fuels, as well as estimate HRR based on gas concentration readings. The main purpose of the parametric study with the presence of waves was to investigate the influence of waves on emissions; this was to see if using the same methods to calculate HRR for wave cases would yield a similar agreement to cases with no waves.

Similar to the meso-scale experiments, the large-scale nature of the CRREL field trials piqued interest in combustion product distribution at different heights above a fire. A sampling point on the superstructure at 2.80 m above the pool was selected as the sampling point. This sampling location was chosen based on the presence of an existing Thermocouple (TC), which allowed for gas emission data to be compared to temperature data during data analysis. The superstructure



above the pool will be referred to as TC tree in the subsequent text; this sampling point is denoted as OGES TC tree.

EPA was present for several burn experiments to perform burn emission sampling with the aid of a crane at locations much higher than the TC tree. In light of this, another sampling point was added in the crane to provide an additional data set for the WPI studies and collaborate with EPA data when needed, denoted OGES Crane. The concept of crane sampling is similar to the studies by Tukaew [12] and Tukaew et al. [13]. However, fixating the sampling point on the crane was only made possible as a result of decreased size and weight of the new OGES.

To visualize the overall setup, Fig. 6a shows an overview of the layout at CRREL, while Fig. 6b is a side view. The sampling tube for OGES TC tree was connected to the filter train and gas sensor module located within a control shed next to the wave tank. In addition, this control shed housed the data logging equipment for the gas sensor data, temperature data, and controller for the wave tank paddle. On the other side of the wave tank was the EPA station where EPA personnel were situated during burn experiments to monitor data streams. Figure 7a shows an overview photo of the wave tank; Fig. 7b shows a detailed photo of the OGES TC tree sampling point. The OGES Crane sampling point, as shown in Fig. 8, was connected via sampling tube to gas sensor data logging equipment located in the EPA station. Table 1 summarizes the locations of the sampling points relative to the fuel surface.

A source of concern would be the difference in tube length, especially the TC tree sampling point versus the crane sampling point, which would result in different time delays recorded by the data logging equipment. This concern was alleviated by comparing the gas sensor data to the temperature data to consider the amount of time delay within the sampling lines.

Out of five total experiments, EPA personnel and the crane operator were only present for two experiments. For subsequent experiments, a zip line was mounted at the facility to mimic the crane as much as possible. The OGES Crane sampling point was fixed to this zip line at a height of 4.00 m above the pool surface, the highest possible height at this facility. A string of metal wire was used to pull OGES Crane along the zip line to maintain its presence within the smoke plume during wind shifts. The location of the zip line is shown in Fig. 6.

A more detailed photograph of the sampling point for OGES Crane as well as the sampling rigs used by EPA, called the Flyer, is shown in Fig. 8. The OGES sampling tube is fixated on an aluminum frame next to the Flyer, while its tip is reinforced with a barbed metal hose connector to ensure the tip does not deform and collapse in the case of higher temperatures when the crane moves to close proximity of the flames. The Flyer was developed in-house by EPA and can measure CO<sub>2</sub>, CO, PM<sub>2.5</sub> (particulate matter of mass median diameter 2.5 μm or less), Black Carbon (BC), total carbon/organic carbon/elemental carbon (TC/OC/EC), polycyclic aromatic hydrocarbons (PAHs), volatile organic compounds (VOCs), and polychlorinated dibenzo-p dioxins/polychlorinated dibenzofurans (PCDD/PCDF) from the smoke plumes. The main goal of EPA was to study the accumulation of toxic gases and particulates throughout a burn experiment. As shown in

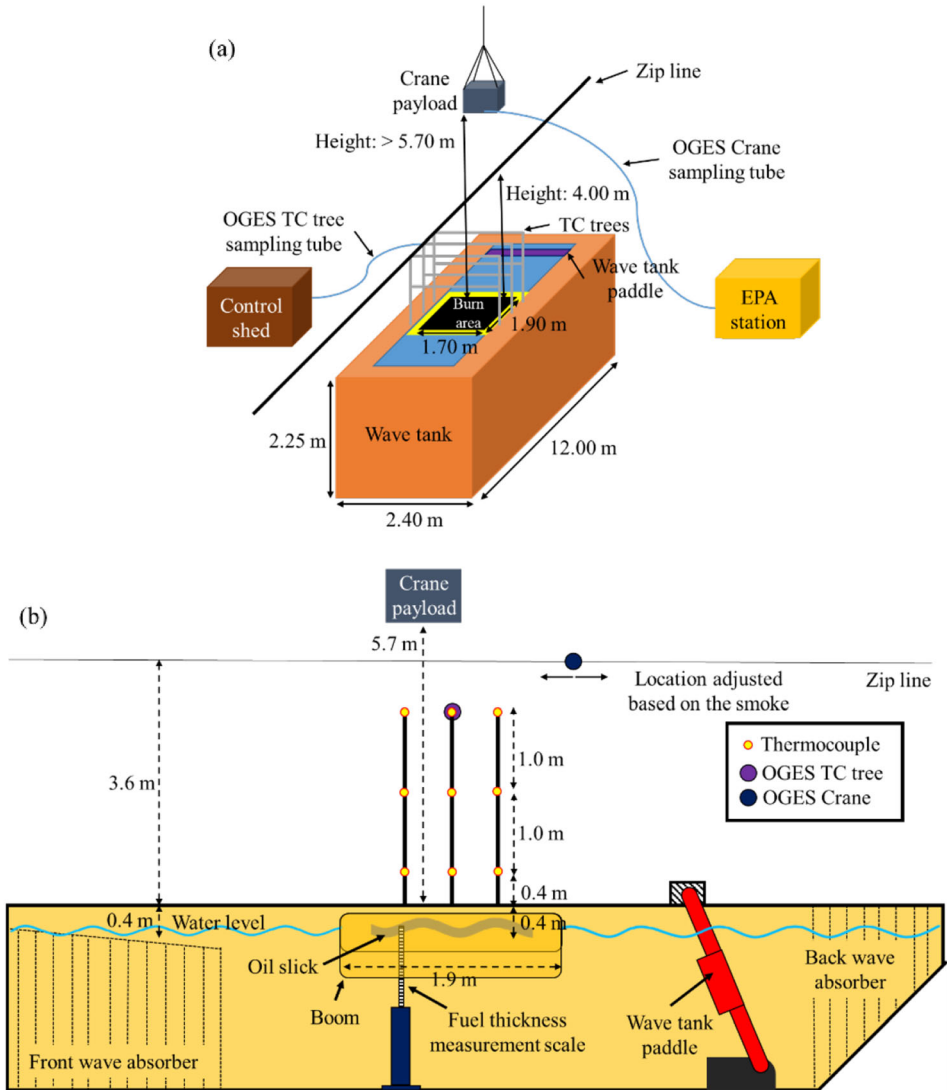


**Figure 6. Diagram of layout and OGES connections at CRREL, a overview; b side view.**

the previous figure, the sampling instrumentation was suspended and maneuvered via crane into the smoke plume with guidance from the Flyer's operator, who monitored real-time temperature and CO<sub>2</sub> levels. In particular, this study compared measured CO<sub>2</sub> and CO values with EPA.

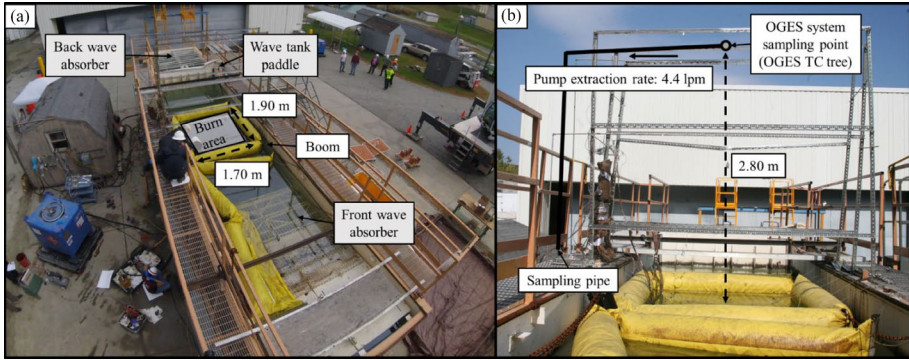


**Figure 7. OGES setup on CRREL wave tank, a overview photo, b detailed photo.**

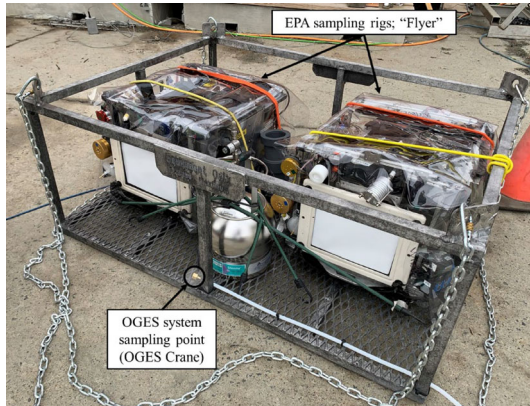


**Figure 8. Detailed depiction of OGES and EPA setup on the crane.**

**Table 1  
OGES sampling points for CRREL experiments**

OGES sampling point	Location
TC tree	Height: 2.80 m Position: Centerline
Crane	Varies: Crane operator attempts to maintain payload within smoke plume as much as possible

## 2.4. Meso-Scale Versus Large-Scale Experiments

This study involved two different setups, one at the meso-scale in an indoor laboratory environment at WPI, the other at the large-scale in an outdoor environment at CRREL. However, regardless of scale, both sets of experiments are inherently similar in that they are both pool fires. However, the large-scale experiments had three additional variables. The first one was the presence of a large body of water beneath the oil; the second was the addition of waves; the third was the presence of wind and changes in wind direction. These were not included in the meso-scale experiments. Diagrams from Fig. 9 provide a summary of the pool fire sizes as well as the sampling heights of the gas analysis equipment.

## 3. Results and Discussion

### 3.1. Meso-Scale 75 cm Indoor Experiments

**3.1.1. Combustion Product Spatial Distribution** Figure 10 shows the vertical distribution along the centerline for CO<sub>2</sub> and CO emissions for the meso-scale 75 cm burn experiments. Figure 10(a) shows the results for ANS crude oil and Fig. 10(b) for 87-octane gasoline. Heights below 1.00 m were omitted for being in too close proximity to the base of the fire, yielding concentrations that exceeded the capabilities of the gas sensors and industrial gas analyzers. The shaded regions correspond to the intermittent zone defined by McCaffrey [15, 21]. This will be important in a later discussion regarding HRR.

Interestingly, trends for both types of fuels are similar with respect to vertical distance from the pool surface, but the trends between CO<sub>2</sub> and CO are drastically different. Observations for both ANS crude oil and 87-octane gasoline show concentration of CO<sub>2</sub> seems to decrease in a relatively linear fashion with respect to height, while CO concentration decreases exponentially. Since this trend is consistent for both types of fuel, observations suggest this trend is species-specific and

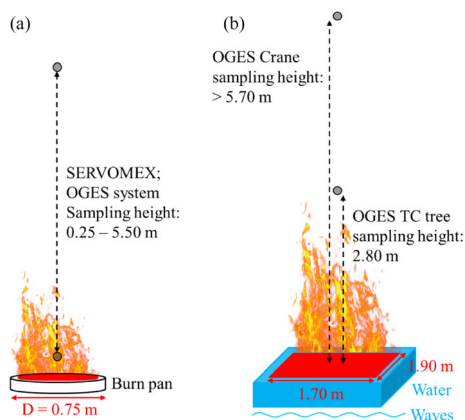


**Figure 9. Diagrams summarizing the different pool fires used in this study at a meso-scale and b large-scale.**

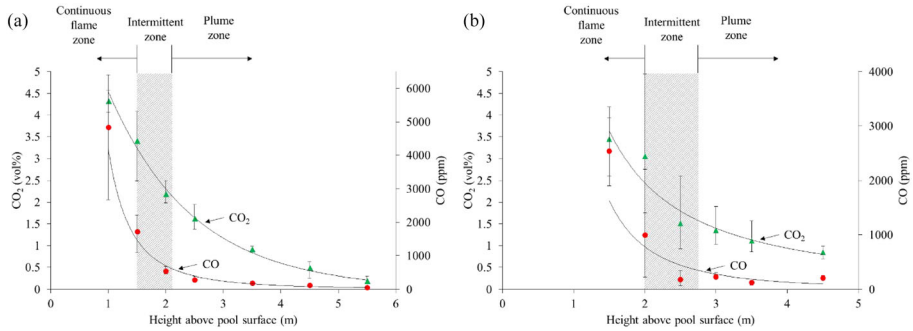


**Figure 10. Vertical distribution of CO<sub>2</sub> and CO concentrations within the smoke plume of 75 cm pool fire, a ANS crude oil; b 87-octane gasoline. Error bars represent the variation of measured concentrations among the three repeat tests.**

not fuel-specific. For other harmful combustion products, such as nitrogen oxides (NO<sub>x</sub>) and sulfur oxides (SO<sub>x</sub>), which were not measured in this study, it is currently unknown whether these gas species diffuse in a manner that is similar to CO<sub>2</sub> or CO. Future studies on combustion product sampling can include measurements of these additional gas species to achieve an improved understanding of diffusion for specific gas species. This is elaborated further in the large-scale experiments at CRREL when discussing the validity of OGES TC tree and OGES Crane data.

**3.2. CO/CO<sub>2</sub> Ratio**

Another method for burning behavior analysis is the comparison of CO/CO<sub>2</sub> ratio. Before comparing between data sets, the CO/CO<sub>2</sub> ratios at different heights along the centerline of a smoke plume should be evaluated to determine the opti-

**Table 2  
Average CO/CO<sub>2</sub> ratio at different heights above pool surface for 75 cm indoor pool fire experiments with two different fuels**

Height above pool surface (m)	ANS crude oil	87-Octane gasoline
1.0	0.1119 ± 0.0307	
1.5	0.0504 ± 0.0042	0.0736 ± 0.0011
2.0	0.0245 ± 0.0015	0.0327 ± 0.0131
2.5	0.0173 ± 0.0017	0.0121 ± 0.0025
3.0		0.0169 ± 0.0009
3.5	0.0201 ± 0.0032	0.0116 ± 0.0011
4.5	0.0233 ± 0.0105	0.0241 ± 0.0004
5.5	0.0253 ± 0.0042	

mal sampling point above a fire that will serve as a basis for further burning behavior analyses. Table 2 and Fig. 11 show the CO/CO<sub>2</sub> ratios for a 75 cm pool fire using ANS crude oil and 87-octane gasoline at the different sampling heights mentioned in the previous section. Normalized plots are shown in Fig. 11 by dividing sampling height over observed flame height.

As indicated in Fig. 5, the flame height for the 75 cm ANS crude oil fire was approximately 1.5 m. Observing CO/CO<sub>2</sub> ratios for ANS crude oil, there is an obvious difference between the values obtained above the flame tip compared to below it. There is a visible decrease in CO/CO<sub>2</sub> ratio above the flame tip at 1.5 m. This can be attributed to the fact that at heights of 1.5 m and below, it is the continuous flame zone, and therefore ongoing flame chemistry is still a significant factor that is affecting the results of emissions sampling. The standard deviation also reflects this as ongoing combustion results in rapid changing of gas species, and therefore sampled gas concentrations show immense fluctuations between repeat tests.

For 87-octane gasoline, Fig. 5 shows the flame height to be approximately 2 m. With that knowledge, a visible cutoff point past the location of the flame tip is observed once again. Similar to the ANS crude oil cases, the standard deviation between repeat tests is much larger for heights in the continuous flame zone, where combustion is ongoing. In contrast, the standard deviation for heights in the plume zone is rather small.

At heights above the flame tip, where only the smoke plume is present and there are no flames, average CO/CO<sub>2</sub> ratios along the centerline of the fire maintain consistent values between 0.0173 and 0.0253. Even at heights where effects from the ambient environment begin to cause significant dilution of the sampled gas species, the standard deviation is rather small between repeat tests compared to locations in the continuous flame zone. Tsuchiya [2] measured and reported CO/CO<sub>2</sub> ratios from experiments performed in an ASTM HRR apparatus and E-84 tunnel for various solid fuels, such as particleboard, asbestos board, and red oak. Values reported in literature indicate that for well-ventilated indoor scenarios, the three solid fuels mentioned above yielded CO/CO<sub>2</sub> ratios between 0.002

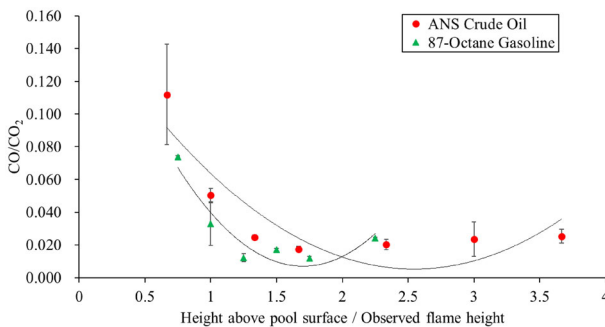


**Figure 11. Summary of CO/CO<sub>2</sub> ratios for 75 cm indoor pool fire experiments with two different fuels. Error bars represent the variation among the three repeat tests.**

and 0.300. The CO/CO<sub>2</sub> ratios obtained in this study show consistency with values reported by Tsuchiya.

CO/CO<sub>2</sub> ratios maintain consistent values above the flame tip; however, observations show the value begins to deviate when the normalized height, or height above pool surface divided by observed flame height, exceeds 2. The hypothesis from observations is that CO concentration decays exponentially with height, while CO<sub>2</sub> concentration decays in a relatively linear fashion. At heights exceeding two times the flame height, rapid dilution of CO gas may yield results that are not representative of the actual burning behavior.

Using the crude oil and gasoline data sets as a baseline, the optimal sampling heights for meso-scale experiments should be above the flame tip but no more than two times that of the observed flame height. This ensures only gas emissions from the smoke plume are sampled but the effects from ambient dilution are minimized, particularly for CO. This corresponds to the intermittent and plume regime of the McCaffrey plume [15].

### 3.3. Large-Scale Outdoor Experiments at CRREL

Five burn experiments were performed at CRREL. The first three experiments were performed using HOOPS crude oil to compare between a baseline case and two wave profiles. The latter two experiments consisted of bunker fuel, as well as a third wave profile.

Densities for HOOPS crude oil and bunker fuel were 784 kg/m<sup>3</sup> and 940 kg/m<sup>3</sup> respectively. The three wave profiles are described using wave period and wave height. Wave 1–2.5 s, 7 cm; Wave 2–4 s, 14 cm; Wave 3–1 s, 4 cm.

### 3.4. OGES TC Tree Data

OGES TC tree was 2.8 m above the surface of the pool and located at the center-line of the fire. Table 3 is a summary of the combustion product measurements sampled by OGES TC tree throughout the five experiments. For the case of CO<sub>2</sub>, the value is reported after deducting 0.046 vol% from the measured concentration. Deduction of this value from the measured concentration is to account for the initial ambient CO<sub>2</sub> concentration, which averaged 460 ppm, or 0.046 vol%, during the experiments. This yields the amount of CO<sub>2</sub> produced from the fire. In practice, this value is very small and this subtraction can be neglected, however, it is included in this study for completeness. For CO, the ambient value is 0 ppm. Since there is a consumption of O<sub>2</sub> instead of production, the reported value is obtained after deducting the measured O<sub>2</sub> concentration from the measured ambient value of 20.80 vol%.

In Table 3, peak values represent the peak amount of gas concentration measured by OGES. For CO<sub>2</sub> and CO, it represents the peak amount produced. In the case of O<sub>2</sub>, it represents the peak amount consumed. Average (Avg) values represent sampled gas concentrations averaged over the entire burn.

Figure 12 shows the CO<sub>2</sub>, CO, and O<sub>2</sub> concentration curves throughout the entirety of the burn for the first three experiments sampled from by OGES TC

**Table 3**  
**Summary of combustion product concentrations measured at 2.8 m above pool surface**

Fuel	Initial thickness (cm)	Wave number	Peak/Avg produced CO <sub>2</sub> (vol%)	Peak/Avg produced CO (vol%)	Peak/Avg consumed O <sub>2</sub> (vol%)	Soot <sup>^</sup> (g)	Regression rate (mm/min)	Burn time (min)	Burn efficiency (%)
HOOPS	8		4.637/1.415	0.460/0.098	7.500/2.081	0.01	1.54	30.0	57
HOOPS*	8	Wave 1	4.540/1.817	0.475/0.118	7.834/2.946	0.10	1.86	42.0	95
HOOPS	8	Wave 2	2.798/1.137	0.299/0.054	5.331/1.685	0.01	1.45	54.0	97
Bunker	1		1.943/0.705	0.106/0.035	2.797/1.107		1.25	5.5	74
Bunker	1	Wave 3	1.122/0.405	0.053/0.019	1.523/0.653	0.02	1.72	6.0	86

\*Rainy day

<sup>^</sup> Fine particle filter in Fig. 1



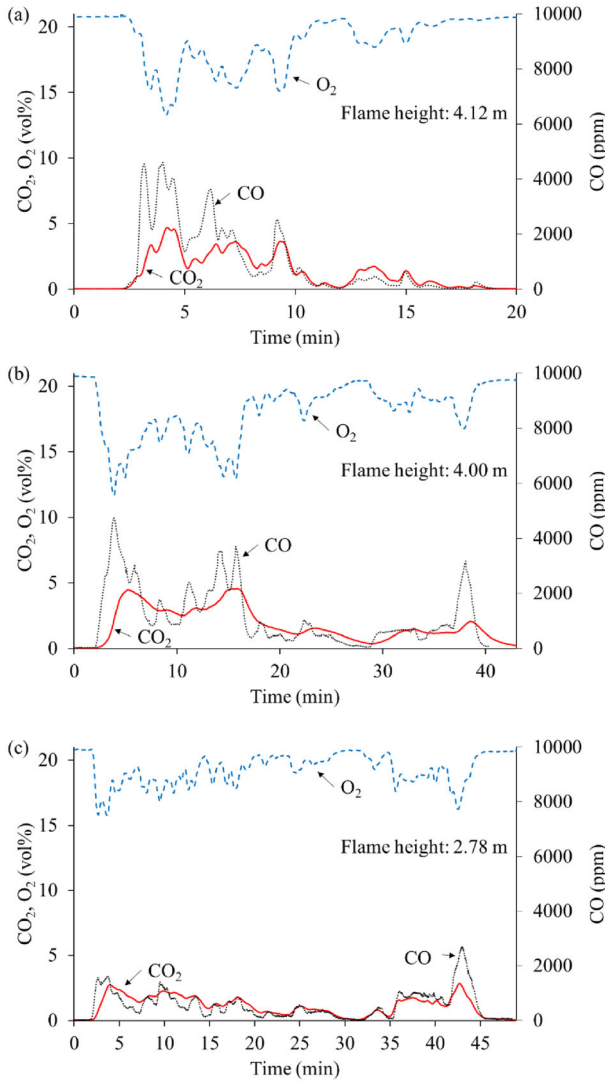


**Figure 12. CO<sub>2</sub>, CO, and O<sub>2</sub> concentration curves throughout the entirety of the burn experiment at 2.8 m along centerline, a HOOPS crude oil without wave; b HOOPS crude oil with Wave 1; c HOOPS crude oil with Wave 2.**

tree at 2.8 m above the pool surface. The plots shown were readings from the portable gas sensors.

Figure 13 provides timeline photographs to explain the gas concentration curves for Fig. 12c. At 1 min, there is a very tall initial flame height. This is attributed to the lighter components in the crude oil being burned off in the early stages of the fire. The CO<sub>2</sub> and CO values reflect this as there is a peak at the start of the fire.

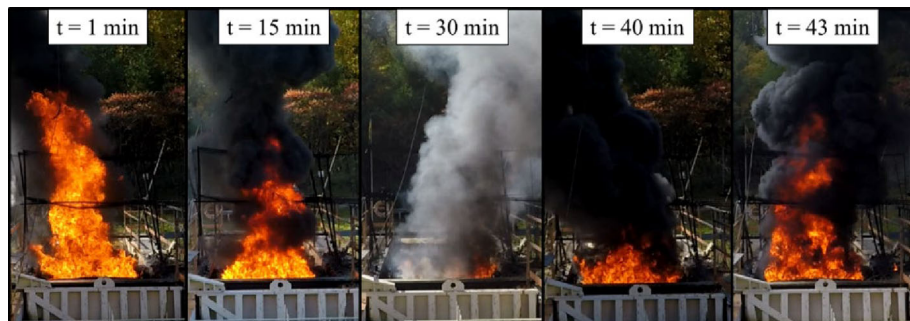


**Figure 13. Timeline photograph of HOOPS crude oil with Wave 2. Flame heights concur with measured gas concentrations at corresponding time stamps.**

At 10 min, the flame height has decreased slightly because the fire is now burning heavier components. There is a corresponding decrease in  $\text{CO}_2$ , however,  $\text{CO}$  values have increased because heavier components tend to have a higher degree of incomplete combustion. At 30 min, oil foaming from boiling water below the oil causes the flames to extinguish temporarily. However, the foam breaks down after a few minutes and the surrounding residual flames allow reignition of the entire pool to occur. At 40 min, there is a steady flame, but the smoke is much thicker and darker compared to earlier photos. At 43 min, the fuel slick is now very thin and allows boilover to occur, resulting in a very tall flame for a short period before complete extinction of the fire.

### 3.5. OGES Crane Data

For the first two experiments, EPA utilized a crane to collect data regarding emissions from outdoor pool fires, specifically particulate matter (PM) and volatile organic compounds (VOC). Similar to this study, EPA also sampled  $\text{CO}$  and  $\text{CO}_2$  concentrations throughout the burn. For three experiments, the crane was not present and the zip line was used, as shown in Fig. 6. Table 4 is a summary of the combustion product measurements sampled at a height of 4.00 m (zip line) or around 5.70 m (crane) throughout the five experiments. The measurements were not made along the centerline but followed the plume trajectory.

As noted in Fig. 6 in the experimental setup section, the crane was not static. The crane operator would maneuver the crane to allow for the sampling point to be completely engulfed by the smoke plume depending on the direction of the wind. However, as seen from Table 4, this was not without its challenges. Initially, the crane operator required some repetitions to maintain the sampling apparatuses within the smoke plume. In addition, obstruction from the dark smoke limited visibility and required external communication. This caused slight delays, which would result in gaps of missing data points during sudden wind shifts. Because of this, an average value for the combustion product concentrations could not be reasonably calculated for the first experiment.

**Table 4**  
**Summary of combustion product concentrations measured by OGES Crane**

Fuel	Initial thickness (cm)	Wave number	Peak/Avg produced CO <sub>2</sub> (vol%)	Peak/Avg produced CO (ppm)	Peak/Avg consumed O <sub>2</sub> (vol%)	Soot <sup>^</sup> (g)	Regression rate (mm/min)	Burn time (min)	Burn efficiency (%)
HOOPS <sup>a</sup>	8		0.247/	33/	0.117/	0.01	1.54	30.0	57
HOOPS <sup>a*</sup>	8	Wave 1	0.858/0.455	105/34	0.292/	0.10	1.86	42.0	95
HOOPS <sup>b</sup>	8	Wave 2	2.197/0.651	224/50		0.01	1.45	54.0	97
Bunker <sup>b</sup>	1		1.860/0.490	113/49			1.25	5.5	74
Bunker <sup>b</sup>	1	Wave 3	2.146/0.659	1420/460		0.02	1.72	6.0	86

<sup>a</sup>Crane

<sup>b</sup>Zip line

\*Rainy day

<sup>^</sup> Fine particle filter in Fig. 1

Table 4 shows sampled concentrations to be relatively higher when using the zip line compared to the crane. This is because the zip line was situated at a height of 4.0 m above the pool, while the average height for the cases with a crane was approximately 5.7 m. 4.0 m was the highest allowable mounting height for a zip line at the CRREL facility.

However, recall the conclusion from the meso-scale experiments concerning optimal sampling height. It should be above the flame tip but no more than two times that of the observed flame height. Visual observations from video footage showed the average flame height to be around 2.7 m. Since 5.7 m was the minimum height for the crane, it consistently exceeded this value, which resulted in sampling heights that exceeded the optimal range for OGES. Meso-scale experiments showed that CO concentrations decay exponentially with height, diffusing much quicker than CO<sub>2</sub> as height increases. This shows the possibility for skewed results, especially when sampling heights exceed a certain range.

### 3.6. Comparison with EPA Results

As mentioned previously, EPA was only present for the first two experiments, therefore only two cases will be compared to EPA data in this section. Using Modified Combustion Efficiency (MCE) to compare burning behavior for different experiments,

$$MCE = \frac{CO_2}{CO_2 + CO} \quad (1)$$

where CO<sub>2</sub> and CO are in vol%.

MCE is a different way of expressing the CO/CO<sub>2</sub> ratio. In general, a higher CO/CO<sub>2</sub> ratio represents a higher degree of incomplete combustion, while a higher MCE represents the opposite. Both terms can be compared since the included variables are the same. Figure 14 shows a comparison between calculated MCE values obtained from both OGES TC tree and OGES Crane. Both peak and average concentrations values are reported in the figure. EPA values were obtained from the final report [23].

An initial assumption is that increased convective cooling from wave behavior would lower the combustion efficiency of a fire. Interestingly, both EPA and WPI data seem to suggest that the effect of Wave 1 on combustion efficiency is negligible. More observations on the influence of waves are given in the latter HRR discussion.

It is observed that OGES TC tree yielded MCE values that were consistent with the reported values by EPA. Both peak and average concentrations from OGES TC tree produced reasonable results. At the same time, however, one cannot ignore that OGES Crane yielded results that are not in good agreement with other values. It is also noted that the values approach unity, meaning OGES Crane only captured relatively low amounts of CO compared to CO<sub>2</sub>. A possible reason is that wind shifts affected OGES Crane more than OGES TC tree. The fact that OGES TC tree was in much closer proximity to the fire aided in its ability to be

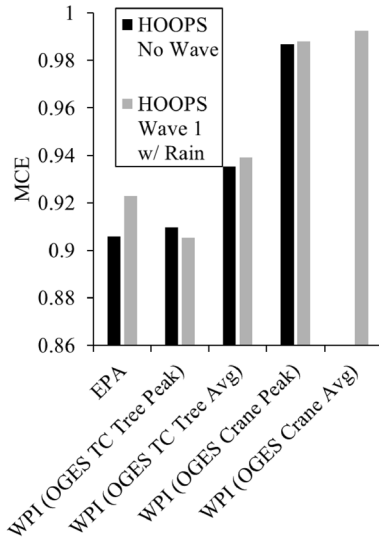


**Figure 14. MCE comparison between WPI and EPA reported values.**

fully engulfed within the smoke plume compared to OGES Crane during wind shifts. Another contributor to uncertainty can be attributed to the same model of CO sensors being used on both OGES TC tree and OGES Crane. The CO sensors were calibrated for higher concentrations upwards of 5000 ppm, but CO concentrations at the average crane height of 5.7 m were in the range of 100 ppm. The sensors likely had less sensitivity at low concentrations.

However, the same report by EPA [23] reported peak CO concentrations of approximately 150 ppm in the same sampling location. The peak CO concentration of 105 ppm sampled by OGES Crane was within a similar range. A reasonable hypothesis stems from the results shown in the meso-scale experiments. CO concentrations show exponential decay with respect to height compared to CO<sub>2</sub> concentrations. This shows that sampling locations that exceed a certain height may yield CO/CO<sub>2</sub> ratios, or MCE values in this case, that are not representative of the actual burning behavior when using these values to predict HRR.

### 3.7. Heat Release Rate (HRR)

Six different methods can be used to calculate the HRR ( $\dot{Q}$ ) or energy release rate of a fire, as shown in Fig. 15.

Of these, this paper uses three methods to calculate HRR: Oxygen Consumption (OC) method, Carbon Dioxide Generation (CDG) method, and Mass Burning Rate (MBR) method. OC method is represented by the product of  $\dot{m}_{O_2}$  and  $\Delta H_{O_2}$ . CDG method is represented by the product of  $\dot{m}_{CO_2}$  and  $\Delta H_{CO_2}$ . In the CRREL experiments, however, sampled CO concentrations were rather high compared to small and meso-scale fires, which represents a larger degree of incomplete combustion. Therefore, considerations for CO production were included in the

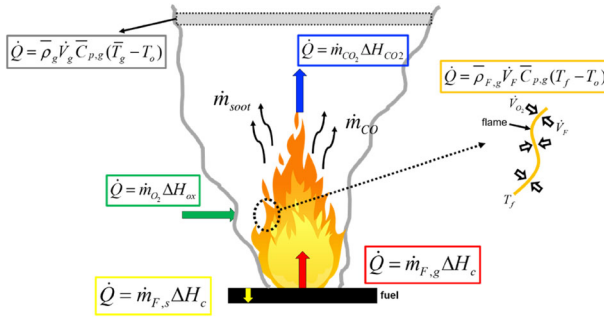


**Figure 15. Six different methods of calculating HRR. The first two methods multiply heat of combustion ( $\Delta H_c$ ) and mass of fuel consumed ( $\dot{m}_{F,s}$ ) or mass of fuel vapor released ( $\dot{m}_{F,g}$ ) per unit time. The third method is based on the amount of consumed oxygen. The fourth method uses produced  $\text{CO}_2$ . The fifth method assumes energy released by combustion is used to heat the gas to a flame temperature at the flame location. The sixth method is based on the temperature rise of the exhaust gases passing through the control volume [24].**

calculations. Regarding the correction term for CO production in the OC method, the detailed procedure is provided in Janssens and Parker [5].

For this derivation, a reaction is assumed where all CO is converted to  $\text{CO}_2$ , as shown in Eq. (2), where the heat release per unit mass of oxygen used to convert CO to  $\text{CO}_2$  ( $\Delta H_{O_2}^{CO}$ ) is 17.6 kJ/g and  $(\Delta \dot{m}_{O_2})_{cor}$  represents the mass flow rate of  $\text{O}_2$  for the oxidation of CO produced [5]. Measurements of OGES are presented as volume fractions of a given gas species within the control volume ( $X_{O_2}$ ,  $X_{CO_2}$ ,  $X_{CO}$ ), therefore these terms need to be present within the equations.



From this,  $(\Delta \dot{m}_{O_2})_{cor}$  can be represented as Eq. (3),

$$(\Delta \dot{m}_{O_2})_{cor} = \frac{1}{2} \dot{m}_{CO} \frac{M_{O_2}}{M_{CO}} = \frac{1}{2} \dot{m}_{O_2} \frac{X_{CO}}{X_{O_2}} = \frac{1}{2} (1 - \phi) \frac{X_{CO} M_{O_2}}{X_{O_2} M_{CO}} \frac{\dot{m}}{1 + \phi(\alpha - 1)} X_{O_2}^0 \tag{3}$$

where the term  $\phi$  is given by

$$\phi = \frac{X_{O_2}^0 (1 - X_{CO_2} - X_{CO}) - X_{O_2} (1 - X_{CO_2}^0)}{(1 - X_{O_2} - X_{CO_2} - X_{CO}) X_{O_2}^0} \tag{4}$$

and  $M_{O_2}$  and  $M_{CO}$  are the molecular weight of  $\text{O}_2$  and CO respectively. Recall that the general assumption for complete combustion is



Using Hess’s Law, the calculated HRR using the OC method is represented as Eq. (6),

$$\dot{Q}_{OC} = \Delta H_{O_2}(\dot{m}_{O_2}^0 - \dot{m}_{O_2}) - (\Delta H_{O_2}^{CO} - \Delta H_{O_2})(\Delta \dot{m}_{O_2})_{cor} \tag{6}$$

Combining Eq. (6) with Eqs. (3) and (4) gives the final form for the OC method with CO correction.

$$\dot{Q}_{OC} = [\Delta H_{O_2}\phi - (\Delta H_{O_2}^{CO} - \Delta H_{O_2})\frac{1 - \phi X_{CO}}{2 \frac{X_{CO}}{X_{O_2}}}] \frac{\dot{m}}{1 + \phi(\alpha - 1) \frac{M_{O_2}}{M_{air}}} X_{O_2}^0 \tag{7}$$

The original expression by Janssens and Parker [5] also includes humidity of air by multiplying the last term in Eq. (7) by  $(1 - X_{H_2O}^0)$ . However, in this study, dry air was assumed and  $X_{H_2O}^0$  was zero.  $M_{air}$  was 29 g/mole, and  $\alpha$  was 1.105 [5].

A study by Brohez [25] analyzed the uncertainty of adding CO and soot correction terms to the OC method. Brohez [25] recommends when burning fuel of unknown chemical composition, crude oil in this instance, the simplest measurement procedure comprising of only O<sub>2</sub> measurement should be used for the OC method, and therefore both CO and soot corrections can be neglected. ASTM E1354 [4] supports this, observing that even a 10 vol% production of CO yielded only about a 2% difference in HRR calculations from the simplest form. The CRREL experiments in this current study showed only a 0.3–1.1% difference in HRR from the simplest form of OC method, which is comparable to the values reported in literature. Although the addition of correction terms is useful for a laboratory setting where accuracy is important, the large-scale and outdoor nature of the CRREL experiments allowed this uncertainty to be deemed negligible.

For the CDG method, the base form is shown as Eq. (8).

$$\dot{Q}_{CDG} = \Delta H_{CO_2}(\dot{m}_{CO_2} - \dot{m}_{CO_2}^0) + \Delta H_{CO}(\dot{m}_{CO} - \dot{m}_{CO}^0) \tag{8}$$

To incorporate these values,  $\dot{m}_{CO_2} = \dot{V}X_{CO_2}\rho_{CO_2}$  is the product of total volume flow rate ( $\dot{V}$ ), volume fraction of CO<sub>2</sub> ( $X_{CO_2}$ ), and density of CO<sub>2</sub> ( $\rho_{CO_2}$ ). A similar procedure can be performed for CO.  $\dot{V}$  can be calculated by dividing total mass flow rate ( $\dot{m}$ ) over the density of air ( $\rho_{air}$ ). From this, the expanded CDG method equation becomes Eq. (9).

$$\begin{aligned} \dot{Q}_{CDG} = \Delta H_{CO_2} & \left( \frac{\dot{m}}{\rho_{air}} X_{CO_2} \rho_{CO_2} - \frac{\dot{m}}{\rho_{air}} X_{CO_2}^0 \rho_{CO_2} \right) + \Delta H_{CO} \left( \frac{\dot{m}}{\rho_{air}} X_{CO} \rho_{CO} \right. \\ & \left. - \frac{\dot{m}}{\rho_{air}} X_{CO}^0 \rho_{CO} \right) \end{aligned} \tag{9}$$

**Table 5**  
**Summary of mass flow rate correlations for a buoyant diffusion flame from McCaffrey [21]**

Regime	$z/\dot{Q}^{2/5}$ (m/kW <sup>2/5</sup> )	Correlation
Continuous flame	< 0.08	$\dot{m}/\dot{Q} = 0.111(z/\dot{Q}^{2/5})^{0.566}$
Intermittent	0.08–0.20	$\dot{m}/\dot{Q} = 0.026(z/\dot{Q}^{2/5})^{0.909}$
Plume	> 0.20	$\dot{m}/\dot{Q} = 0.124(z/\dot{Q}^{2/5})^{1.895}$

**Table 6**  
**Summary of centerline constants for a buoyant diffusion flame from McCaffrey [21]**

Regime	$k$	$\eta$	$z/\dot{Q}^{2/5}$ (m/kW <sup>2/5</sup> )	$C$
Continuous flame	6.8 (m <sup>1/2</sup> /s)	1/2	< 0.08	0.9
Intermittent	1.9 (m/kW <sup>1/5</sup> .s)	0	0.08–0.20	0.9
Plume	1.1 (m <sup>4/3</sup> /kW <sup>1/3</sup> .s)	-1/3	> 0.20	0.9

Equations (7) and (9) show HRR calculations based on OC and CDG methods require knowledge of the total mass flow rate through the control volume. Plume theories derived by Heskestad [11] and McCaffrey [21] were used to estimate mass flow rates along the centerline of the fire at different heights. In addition, profiles of vertical velocity across the horizontal direction of the plume are assumed to be uniform based on integral formulations by Morton et al. [22]. This results in a simplification where a uniform “top hat” profile was used when estimating mass flow rate at a certain height. This assumption also means a radial distribution of CO<sub>2</sub>, CO, and O<sub>2</sub> is not needed.

McCaffrey [15, 21] divides a buoyant diffusion flame into three distinct regimes: continuous flame zone, intermittent zone, and plume zone. Continuous flame zone is the zone where the flame is always present. Intermittent zone is the zone where the eruption and break from the anchored flame with a regular flicker of a few Hz can be observed. Plume zone is the zone above the visible flame where flames are no longer present. The regime is determined based on height above the burner ( $z$ ) and total HRR ( $\dot{Q}$ ). McCaffrey [21] provides equations to calculate mass flow rate ( $\dot{m}$ ) along the centerline of the fire based on the regime, as shown in Table 5.

McCaffrey [15] also provides equations for centerline velocity and temperature of a buoyant diffusion flame, shown as Eq. (10) and (11) respectively. Table 6 shows the constants used for the three distinct regimes.  $u_0$  is centerline velocity;  $g$  is gravitational acceleration, or 9.81 m/s<sup>2</sup>;  $T_0$  is ambient temperature;  $\Delta T_0$  is tem-



perature rise above ambient;  $C$  is an empirical correction factor, or 0.9;  $\eta$  is an empirical exponent coefficient.

$$u_0/\dot{Q}^{1/5} = k(z/\dot{Q}^{2/5})^\eta \quad (10)$$

$$2g\Delta T_0/T_0 = (k/C)^2(z/\dot{Q}^{2/5})^{2\eta-1} \quad (11)$$

The third method of calculating HRR is taking the product of mass burning rate ( $\dot{m}_{F,s}$ ) and heat of combustion ( $\Delta H_c$ ) for a given fuel [3, 25]. Shi et al. [26] report the heat of combustion for crude oil as 44,770 kJ/kg. The mass burning rate (MBR) was calculated based on the average observed regression rate of the fuel layer throughout the experiments. For the meso-scale experiments, this was obtained from load cell data. For the large-scale field experiments, this was obtained by using an underwater camera and the fuel thickness measurement scale shown in Fig. 6b. Further details are available in [27]. Using that as a baseline HRR value, this study calculated HRR based on measured combustion product concentrations.

HRR can also be obtained by using empirical constants reported by Babrauskas [28, 29] for large-scale pool fires,

$$\dot{Q} = \Delta H_c \dot{m}_\infty (1 - e^{-k\beta D}) \times A \quad (12)$$

Equation (12) shows that in addition to the heat of combustion for a given fuel, two additional empirical constants need to be determined. First is the asymptotic mass loss rate per unit area ( $\dot{m}_\infty$ ). The mass loss rate per unit area approaches asymptotic as the pool diameter increase towards infinity. Generally, this equation can be applied to pool fires that are 1 m in diameter or greater. The second constant is the product of extinction-absorption coefficient and beam-length corrector ( $k\beta$ ). However, this correlation yields an HRR value solely based on pool diameter and fuel type, which in this study is identical across cases that use the same fuel. It cannot account for external factors such as waves.

### 3.8. Meso-Scale 75 cm Indoor Experiments

Using Eq. (12) for the meso-scale indoor experiments, a 75 cm ANS crude oil fire would have an HRR of 350 kW, while an 87-octane gasoline fire would be 720 kW. This set of experiments only measured combustion product concentrations. However, the fact that sampling points were located at the centerline allowed for McCaffrey plume correlations [15, 21] to be used to estimate mass flow rate at the sampling point, as shown in Table 5 and Eq. (10) (11). Once these variables were obtained, HRR was calculated using CDG method with measured CO<sub>2</sub> and CO concentrations. Figure 16 shows estimated HRR from CDG method using measured gas concentrations at different heights. The horizontal lines represent HRR approximated by Babrauskas [28, 29] for a 75 cm pool fire.

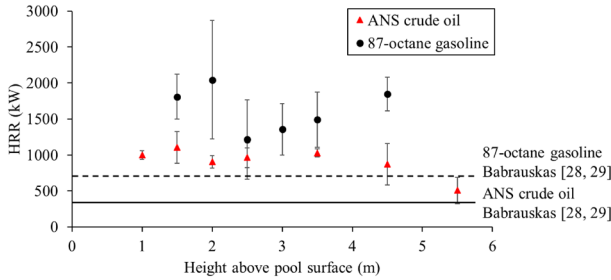


**Figure 16. Estimated HRR for meso-scale 75 cm indoor pool fire experiments. Measured gas concentrations at different heights were used with CDG method to obtain HRR values.**

A sample calculation is provided for HRR calculations using the CDG method. Taking the ANS crude oil case at a height of 2 m above the pool ( $z = 2$  m), which falls into the intermittent flame region of the McCaffrey plume, and using the HRR value of 350 kW by Babrauskas,  $\dot{m} = 2.02$  kg/s can be obtained using the correlations and constants from Table 5. In the case of OGES, it is assumed that the filter train allowed the sampled combustion gases to be lowered to ambient temperature, therefore the densities for specific gas species at 20 °C were used:  $\rho_{air} = 1.20$  kg/m<sup>3</sup>,  $\rho_{CO_2} = 1.84$  kg/m<sup>3</sup>, and  $\rho_{CO} = 1.17$  kg/m<sup>3</sup>. From Fig. 10, the average measured CO<sub>2</sub> and CO concentrations were 2.180 vol% and 534 ppm respectively. Ambient CO<sub>2</sub> and CO concentrations were measured to be 0.046 vol% and 0 ppm respectively.  $\Delta H_{CO_2}$  and  $\Delta H_{CO}$  are 13.3 and 11.1 kJ/g respectively. Using Eq. (9),

$$\begin{aligned} \dot{Q}_{CDG} &= (13,300 \text{ kJ/kg}) \cdot \left[ \left( \frac{2.02}{1.20} \text{ m}^3/\text{s} \right) \cdot (0.02180) \cdot (1.84 \text{ kg/m}^3) - \left( \frac{2.02}{1.20} \text{ m}^3/\text{s} \right) \right. \\ &\quad \cdot (0.00046) \cdot (1.84 \text{ kg/m}^3) \left. \right] + (11,100 \text{ kJ/kg}) \cdot \left[ \left( \frac{2.02}{1.20} \text{ m}^3/\text{s} \right) \cdot (0.00053) \right. \\ &\quad \cdot (1.17 \text{ kg/m}^3) - \left( \frac{2.02}{1.20} \text{ m}^3/\text{s} \right) \cdot (0) \cdot (1.17 \text{ kg/m}^3) \left. \right] \\ &= 908 \text{ kW}. \end{aligned}$$

This value concurs with the value presented in Fig. 16 for ANS crude oil at 2 m above the pool surface.

From Fig. 16, it is interesting that using CDG method from OGES measured CO<sub>2</sub> and CO concentrations yielded HRR values that consistently overestimated for both ANS crude oil and 87-octane gasoline when compared to Babrauskas [28, 29] values. Other measurement methods such as oxygen data, temperature data, and fuel regression rate were lacking, so other methods of validation were not present for this set of experiments.

However, the takeaway from these results is that there is a similar trend for calculated HRR with respect to sampling height. In the continuous flame zone (1–1.5 m for ANS crude oil, 1.5–2 m for 87-octane gasoline), the calculated HRR

increases, moving further away from the HRR predicted by existing correlations. However, once in the intermittent zone (1.5–2 m for ANS crude oil, 2–2.5 m for 87-octane gasoline), the calculated HRR values are closer to measured values from literature. Once the plume zone is reached at further distances ( $> 2$  m for ANS crude oil,  $> 2.5$  m for 87-octane gasoline), the HRR calculated by CDG method again begins to deviate farther from the expected value.

There are two conclusions drawn from these observations. First is that multiple sampling points are needed to achieve a better understanding of the total mass flow rate of the plume. The second is that when multiple points are not possible, the sampling location of gas emissions should be performed in the intermittent zone of the fire, as that yields values that are closest to plume theory correlations.

### 3.9. Large-Scale Outdoor Experiments at CRREL

Based on Eq. (12), HRR is estimated to be 6.2 MW for HOOPS crude oil. Babrauskas [28] does not report values for bunker fuel specifically, but it is stated that bunker fuel falls under the category of heavy fuel oil. Using the constants for heavy fuel oil, the estimated HRR for bunker fuel is 4.3 MW. As stated previously, this correlation yields an HRR value solely based on pool diameter and fuel type, which means an identical HRR will be obtained across cases that use the same fuel. However, this is not the case with external factors such as waves and is one of the limitations of this correlation.

As mentioned in previous sections, this study utilized existing plume theories such as McCaffrey plume [15, 21] to estimate mass flow rate, velocity, and temperature along the centerline at the sampling height, as shown in Table 5 and Eq. (10) (11). Once these variables were obtained, HRR was approximated using CDG method with measured  $\text{CO}_2$  and CO concentrations, or OC method with  $\text{O}_2$  and CO concentrations. Recall that OGES TC tree was located along the centerline of the fire at 2.8 m above the pool surface. This is why McCaffrey plume could be used to obtain variables not measured in this study. However, for the same reason, HRR could not be obtained using OGES Crane data, since the crane was not always situated along the centerline of the plume. HRR calculations were performed similarly to the sample calculations presented in Sect. 3.3.1.

Based on the three distinct flame regimes from McCaffrey [15, 21], Table 5 shows that OGES TC tree was located in the intermittent zone for all five experiments. MBR provided a baseline value for HRR calculation; the value was then used to estimate the mass flow rate along the centerline using Table 5.  $X_{\text{O}_2}$ ,  $X_{\text{CO}_2}$ , and  $X_{\text{CO}}$  were obtained from OGES TC tree measurements, after which these values were used to calculate HRR using OC and CDG method.

Initially, HRR was calculated using OC and CDG methods respectively using both peak and average gas concentration values. However, results showed using peak gas concentrations sampled by OGES did not yield HRR values that were in good agreement with the HRR based on MBR. Using peak values consistently resulted in a significant overestimation of HRR. However, average gas concentration values yielded HRR values that were much more reasonable for this fire size. This made sense, as the MBR was calculated based on an average regression rate

of the fuel layer. For the three cases with HOOPS crude oil, HRR based on MBR was in good agreement with the two HRR values predicted by OC and CDG method within a reasonable degree of error when average gas concentrations were used. Figure 17 shows calculated HRR values using the different methods; HRR calculated using peak gas concentrations are omitted.

Similar to the comparison with EPA data, both MCE (Eq. (1)) and HRR calculations seem to suggest that a fast but short wave like Wave 1 allows more complete combustion of the fire. However, a slow but tall wave like Wave 2 causes HRR to decrease. Regardless of the wave, OGES shows the capability to capture combustion products and effectively estimate HRR based on OC and CDG methods even with the presence of waves. Quantification of waves is out of the scope of this study, but future research is needed to quantify the effect of waves on oil slicks burning above water.

It is interesting to observe that these same methods underestimate HRR for bunker fuel by a considerable margin. For bunker fuel, this suggests a thin fuel layer of 1 cm allows for very fast heat penetration to the water sublayer under the fuel, which promotes burning phenomena such as boilover as the water reaches its boiling point. The boiling water in conjunction with the waves atomizes the fuel quicker since the fuel slick thickness is very thin initially; this enhances the burn rate compared to a calm scenario. The hypothesis of why OC and CDG methods are underestimating the HRR is that the vaporizing water content is a significant component in the flue gases and should be quantified in further studies to more accurately predict HRR using point sampling.

Although currently limited to certain fuels, OGES has demonstrated a low-cost but effective alternative to expensive industrial gas analyzers for HRR estimation, especially in large-scale outdoor fire scenarios where complete encapsulation of the plume is unfeasible and only point sampling is possible. Further refinement of this

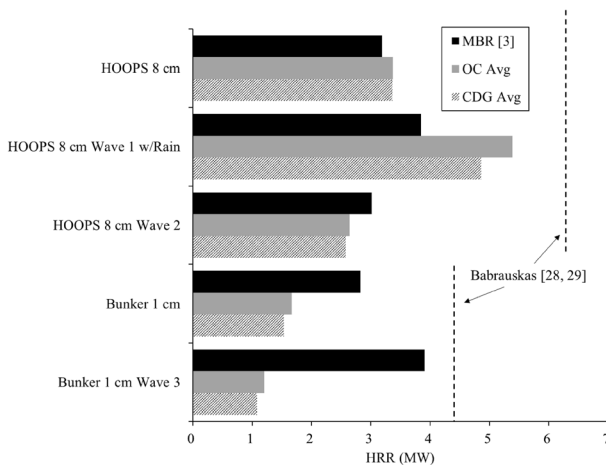


**Figure 17. Comparison of four HRR calculation methods for five experiments at CRREL.**

system, such as measurement of mass flow rate at the sampling location and quantification of water vapor content, can allow it to become applicable for a wider range of fuels.

#### **4. Conclusion**

This study provides new data on burning dynamics of meso and large-scale oil slick fires with and without waves using an Outdoor Gas Emission Sampling (OGES) system. Several improvements, with cost, weight (portability), and measurement capability compared to an earlier design of OGES [12] are also discussed.

Unlike standard calorimeters that sample the entire fire plume using a large exhaust hood, OGES relies on point sampling of  $O_2$ ,  $CO_2$ , and  $CO$  at strategic locations within the plume. These measurements are coupled with plume correlations (McCaffrey [15, 21], Heskestad [11]) to estimate the average mass of air entrained in the horizontal plane where sampling is performed, and calculate the heat release rate (HRR) using Oxygen Consumption (OC) or Carbon Dioxide Generation (CDG) method. Experiments show good agreement with HRR calculated from the average mass loss rate. Further, Modified Combustion Efficiency (MCE) calculated independently by EPA for the large-scale oil slick fires also compare reasonably well with OGES. Additional measurements on  $NO_x$ ,  $SO_x$ , and unburned carbon would further improve the accuracy of OGES and is a pathway for future research.

The meso-scale experiments show that the concentration of  $CO_2$  varies linearly in a vertical height along the plume centerline between 2 to 7D where D is the pool diameter. This region, which falls in McCaffrey's intermittent plume region [15, 21], is advantageous for point-based sampling, particularly using the CDG method.

With high soot-producing fuel like bunker fuel, the HRR is underestimated with OGES. This requires further research especially with future experiments designed with additional sampling points located radially. However, at present, the OGES system has shown to be a low-cost but effective way to measure HRR in large-scale outdoor fire scenarios where traditional hood-based calorimetry methods are not possible.

#### **Acknowledgements**

This study is funded by the Bureau of Safety and Environmental Enforcement, US Department of the Interior, Washington, D.C., under Contract Number 140E0119C0001. The contents do not necessarily reflect the views and policies of the BSEE, nor does mention of the trade names or commercial products constitute endorsement or recommendation for use.

## References

1. Babrauskas V, Peacock RD (1992) Heat release rate: the single most important variable in fire hazard. *Fire Saf J* 18(3):255–272. [https://doi.org/10.1016/0379-7112\(92\)90019-9](https://doi.org/10.1016/0379-7112(92)90019-9)
2. Tsuchiya Y (1982) Methods of determining heat release rate: state-of-the-art. *Fire Saf J* 5(1):49–57. [https://doi.org/10.1016/0379-7112\(82\)90006-6](https://doi.org/10.1016/0379-7112(82)90006-6)
3. Drysdale DD (2016) Thermochemistry. In: Hurley MJ, Gottuk DT, Hall JR (eds) et alSFPE handbook of fire protection engineering Springer, New York, pp 138–150
4. ASTM E1354-16a (2016) Standard test method for heat and visible smoke release rates for materials and products using an oxygen consumption calorimeter. ASTM International, West Conshohocken, PA
5. Janssens M, Parker WJ (1992) Oxygen consumption calorimetry. In: Babrauskas V, Grayson SJ (eds) Heat release in fires Elsevier Applied Science, London, pp 31–60
6. Huggett C (1980) Estimation of rate of heat release by means of oxygen consumption measurements. *Fire Mater* 4(2):61–65. <https://doi.org/10.1002/fam.810040202>
7. Bryant R, Bundy M (2019) The NIST 20 MW calorimetry measurement system for large-fire research, Technical Note (NIST TN). National Institute of Standards and Technology, Gaithersburg
8. Khan MM, Tewarson A, Chaos M (2016) Combustion characteristics of materials and generation of fire products. In: Hurley MJ, Gottuk DT, Hall JR (eds) et alSFPE handbook of fire protection engineering Springer, New York, pp 1143–1232
9. Cooper LY (1994) Some factors affecting the design of a calorimeter hood and exhaust. *J Fire Prot Eng* 6(3):99–111. <https://doi.org/10.1177/104239159400600301>
10. Evans DD, Mulholland GW, Baum HR, Walton WD, McGrattan KB (2001) In situ burning of oil spills. *J Res Nat Inst Stand Technol* 106(1):231–278. <https://doi.org/10.6028/jres.106.009>
11. Heskestad G (1984) Engineering relations for fire plumes. *Fire Saf J* 7(1):25–32. [https://doi.org/10.1016/0379-7112\(84\)90005-5](https://doi.org/10.1016/0379-7112(84)90005-5)
12. Tukaew P (2017) Outdoor Gas Emission Sampling system: a novel method for quantification of fires in outdoor conditions. MS Thesis, Worcester Polytechnic Institute
13. Tukaew P, Arsava KS, Fields SL, Rangwala AS (2019) Outdoor Gas Emission Sampling system –performance during large scale fire tests in Mobile Alabama. In: Proceedings of the thirty-ninth AMOP = technical seminar on environmental contamination and response, Environment Canada, Halifax, Nova Scotia
14. Lizhong Y, Wenxing F, Junqi Y (2008) Experimental research on the spatial distribution of toxic gases in the transport of fire smoke. *J Fire Sci* 26(1):45–62. <https://doi.org/10.1177/0734904107083632>
15. McCaffrey BJ (1979) Purely buoyant diffusion flames: some experimental results. National Bureau of Standards, Washington, DC
16. Sibulkin M, Malary SF (1984) Investigation of completeness of combustion in a wall fire. *Combust Sci Technol* 40(1–4):93–106. <https://doi.org/10.1080/00102208408923800>
17. Aurell J, Gullett BK (2010) Aerostat sampling of PCDD/PCDF emissions from the Gulf oil spill in situ burns. *Environ Sci Technol* 44(24):9431–9437. <https://doi.org/10.1021/es103554y>
18. Aurell J, Gullett BK, Pressley C, Tabor DG, Gribble RD (2011) Aerostat-lofted instrument and sampling method for determination of emissions from open area sources. *Chemosphere* 85(5):806–811. <https://doi.org/10.1016/j.chemosphere.2011.06.075>
19. Aurell J, Gullett BK, Yamamoto D (2012) Emissions from open burning of simulated military waste from forward operating bases. *Environ Sci Technol* 46(20):11004–11012. <https://doi.org/10.1021/es303131k>

20. Hariharan SB, Farahani HF, Rangwala AS, Dowling JL, Oran ES, Gollner MJ (2021) Comparison of particulate-matter emissions from liquid-fueled pool fires and fire whirls. *Combust Flame* 227:483–496. <https://doi.org/10.1016/j.combustflame.2020.12.033>
21. McCaffrey BJ (1983) Momentum implications for buoyant diffusion flames. *Combust Flame* 52:149–167. [https://doi.org/10.1016/0010-2180\(83\)90129-3](https://doi.org/10.1016/0010-2180(83)90129-3)
22. Morton BR, Taylor GI, Turner JS (1956) Turbulent gravitational convection from maintained and instantaneous sources. *Proc R Soc Lond Ser A* 234(1196):1–23. <https://doi.org/10.1098/rspa.1956.0011>
23. Aurell J, Gullett BK (2021) Analysis of emissions and residue from methods to improve combustion efficiency of in situ oil burns, heat transfer technology: Flame Refluxer. Final Report
24. Rangwala AS, Raghavan V (2022) *Mechanisms of fire: chemistry and physical aspects*. Springer, New York
25. Brohez S (2005) Uncertainty analysis of heat release rate measurement from oxygen consumption calorimetry. *Fire Mater* 29(6):383–394. <https://doi.org/10.1002/fam.895>
26. Shi X, Bellino PW, Rangwala AS (2015) Flame heat feedback from crude oil fires in ice cavities. In: *Proceedings of the thirty-ninth AMOP technical seminar on environmental contamination and response*, Environment Canada, Ottawa, ON, pp 767–776
27. Rangwala A, Arsava K, Sauer NG, Ho H, Nair S, Mahnken G, Kottalgi M (2021) Advancing the maturity of the flame refluxer technology. U.S. Department of the Interior, Bureau of Safety and Environmental Enforcement. Report No.: 1104. Contract No.: 140E0118R0007
28. Babrauskas V (2016) Heat Release Rates. In: Hurley MJ, Gottuk DT, Hall JR (eds) *et al* SFPE handbook of fire protection engineering Springer, New York, pp 799–904
29. Babrauskas V (1983) Estimating large pool fire burning rates. *Fire Technol* 19(4):251–261. <https://doi.org/10.1007/BF02380810>

**Publisher's Note** Springer Nature remains neutral with regard to jurisdictional claims in published maps and institutional affiliations.